(Preprint) AAS 11-125

FLYBY DESIGN USING HETEROCLINIC AND HOMOCLINIC CONNECTIONS OF UNSTABLE RESONANT ORBITS

Rodney L. Anderson* **and Martin W. Lo***

Tour designs using flybys have traditionally been studied using two-body patched conic methods. Previous work has shown that trajectories designed using these techniques and with optimization methods follow the invariant manifolds of unstable resonant orbits as they transition between resonances. This work is continued here by computing heteroclinic and homoclinic trajectories associated with these unstable resonant orbits. These trajectories are used with multiple resonances to design flybys that transition between these resonances in the circular restricted three-body problem without the need for two-body approximations.

INTRODUCTION

Tour designs using flybys have been studied using a variety of different approaches. Historically, they rely heavily on the use of two-body, patched-conic approximations to obtain an initial tour with the use of numerical techniques to compute a final continuous trajectory. Techniques related to this method, such as V_∞ leveraging,[1] have been used to approach this problem for some time, and they continue to be developed.[2,3] One of the primary areas of interest for tour design in recent years has been for a Europa orbiter mission. Sweetser et al.[4] and Johannesen and D'Amario[5] primarily combined two-body analyses with numerical techniques to produce potential trajectories traveling to Europa, and they emphasized the importance of what they termed the endgame problem. Various definitions exist for the endgame problem, but for these designs it typically involves transitioning through the last several resonances using Europa down to approach or capture around the moon. More recent work has started incorporating the use of three-body parameters, such as Tisserand's criterion, into the analysis.[6–8] Kloster, Petropoulos, and Longuski, addressed this problem more recently by using elements of the three-body problem in the form of Tisserand graphs.[9]

Alternatively, researchers have examined the problem from a dynamical systems perspective in terms of resonance transitions in the three-body problem. Bollt and Meiss[10] applied dynamical systems theory directly within the three-body problem using the recurrence properties of chaotic dynamics to search for Earth-Moon transfers. Schroer and Ott[11] reduced the transfer time for such problems by targeting the invariant manifolds of unstable resonant orbits. Resonance transition has also been examined from the perspective of comet transitions by a number of researchers. Belbruno and Marsden proposed that the weak stability boundary could explain these transitions.[12] Lo and Ross then suggested that invariant manifolds might play a role in this problem[13] which was subsequently verified by Koon, Lo, Marsden, and Ross.[14] In this work the heteroclinic connections between libration orbits were used to explain the resonance transitions. Howell, Marchand, and Lo then numerically verified this transition mechanism.[15] Additional researchers have found the computation of unstable resonant orbits in general to be useful. Lantoine, Russell, and Campagnola used unstable resonant orbits in the three-body orbits as initial guesses for optimization algorithms to compute resonance transitions, although their algorithm did not include computation of the invariant manifolds.[16] Ross and Scheeres examined the problem in terms of resonance transition using an energy kick function to approximate the effect of gravity flybys.[17]

In our previous work, we showed that impulsive trajectories originally designed using two-body techniques[18–20] and low-thrust trajectories designed using optimization tools[21,22] produced trajectories that closely followed the invariant manifolds of unstable resonant orbits. These manifolds acted as pathways between resonances that the trajectory could follow at different energies. Our work has shown that trajectories designed

*Member of Technical Staff, Jet Propulsion Laboratory, California Institute of Technology, 4800 Oak Grove Drive, M/S 301-121, Pasadena, CA 91109

using two-body approximations and then made continuous in the circular restricted three-body problem (CRTBP) follow the invariant manifolds of unstable resonant orbits as they transition between resonances.[23] It has been further verified by direct computation for single cases that these unstable manifolds possess homoclinic[23] and heteroclinic[24] connections that act as trajectories that transition between resonances.

As can be seen from these descriptions, the flyby problem has been approached with a variety of different methods. Many of these methods are based on numerical techniques or require approximations beyond those made in the CRTBP. In essence, these types of methods are somewhat removed from the actual dynamics. The method presented here follows our previous work and directly computes the invariant manifolds of unstable resonant orbits for resonance transition via homoclinic or heteroclinic connections. Given the current interest in a mission to Europa, these connections are computed for a variety of different resonances in the Jupiter-Europa system. The feasibility of chaining multiple heteroclinic connections together to obtain continuous trajectories is evaluated for use in mission design. It will be shown that this last step requires some small approximations with differential correction, but the majority of the dynamics are apparent until this last minor adjustment. In general this technique provides significant physical insight into the problem as the entire trajectory may be designed visually or geometrically from the dynamics, completely within the CRTBP.

BACKGROUND

Circular Restricted Three-Body Problem

This study focuses on computing trajectories within the CRTBP. Szebehely[25] provides a detailed description of this model, but a brief overview will be given here. In the CRTBP, the goal is to describe the motion of an infinitesimal mass in a system containing two bodies, typically referred to collectively as the primaries, rotating about their center of mass in circular orbits. If the infinitesimal mass is restricted to the plane of motion of the two primaries, the problem is called the planar CRTBP or PCRTBP. The equations of motion are usually formulated in a rotating frame so that the x axis is aligned with the primaries, and dimensionless quantities are used. Using this formulation, the mass of the larger body (the primary) is defined to be $1-\mu$, and the smaller body (the secondary) has mass μ. The primary is located on the x axis at $x_1 = -\mu$, and the secondary is located on the x axis at $x_2 = 1-\mu$. The period of the rotating system is 2π, while the distance between the primaries, the mean motion, and the gravitational constant are all one. The dimensionless time corresponds to the angle between the x axis of the rotating frame and the x axis of the inertial frame. Using this notation, the equations of motion for the infinitesimal mass in the rotating system may be written as

$$\begin{aligned} \ddot{x} - 2\dot{y} &= x - (1-\mu)\frac{x-x_1}{{r_1}^3} - \mu\frac{x-x_2}{{r_2}^3} \\ \ddot{y} + 2\dot{x} &= \left(1 - \frac{(1-\mu)}{{r_1}^3} - \frac{\mu}{{r_2}^3}\right) y \\ \ddot{z} &= -\left(\frac{(1-\mu)}{{r_1}^3} + \frac{\mu}{{r_2}^3}\right) z. \end{aligned} \tag{1}$$

Here, the distances from the infinitesimal mass to the primary and secondary are r_1 and r_2, respectively. An energy-like integral of motion exists in this model called the Jacobi constant, which varies when maneuvers are performed. It may be computed as

$$C = x^2 + y^2 + \frac{2(1-\mu)}{r_1} + \frac{2\mu}{r_2} - \dot{x}^2 - \dot{y}^2 - \dot{z}^2. \tag{2}$$

For particular Jacobi constants there are positions where the resulting velocity is imaginary. A spacecraft cannot travel into these forbidden regions, and the curve bounding them is referred to as a zero velocity curve. Finally, there are five equilibrium points in the problem (the Lagrange points) about which periodic orbits exist. The existence of symmetries in the CRTBP were used when applicable to reduce the computational time required for this analysis. Specifically, it is known that if $(x, y, z, \dot{x}, \dot{y}, \dot{z}, t)$ is a solution in the CRTBP, then $(x, -y, z, -\dot{x}, \dot{y}, -\dot{z}, -t)$ is also a solution.[25] In other words, if a trajectory is reflected about the x axis, a valid trajectory is obtained by traveling along the reflected trajectory in reverse. This property was used to compute the stable manifolds from the unstable manifolds when it was applicable in the following analysis.

Resonant Orbits

A major focus of this analysis was the computation of resonant orbits and their invariant manifolds. In the two-body problem, a spacecraft is periodic in the rotating frame if a spacecraft travels around the primary p times for every q times the secondary travels around, given that $p, q \in \mathbb{N}$. The relationship between the resonant integers, mean motions, and periods of the spacecraft and the smaller primary may be written respectively as

$$\frac{p}{q} = \frac{n_p}{n_q} = \frac{T_q}{T_p}. \tag{3}$$

The mean motion of the smaller primary (n_q) in the CRTBP is unity, so one criterion for the spacecraft to be periodic in the synodic frame is that $n_p = p/q$.

As mentioned previously, the dimensionless period of the smaller primary is 2π, and the configuration repeats itself after q revolutions of the smaller primary. So the period of the infinitesimal mass in the rotating frame is $2\pi q$. Note that in this paper, the form p:q is used for the resonances, which is equivalent to [Europa period]:[spacecraft period] or [spacecraft revolutions]:[Europa revolutions]. Note that the period of the spacecraft in the rotating frame is subsequently denoted by $\mathbb{P}_{sc}$, while Europa's period in the inertial frame is referred to as $\mathbb{P}_e$. In the three-body problem the periods of the spacecraft and the secondary are no longer related precisely by resonant integers, so the definition of mean motion resonance given by

$$pn_p \approx qn_q \tag{4}$$

from Murray and Dermott[26] may be used. In this case, the infinitesimal mass does not quite return to the same point after q revolutions of the secondary, and it is useful to use Poincaré sections to search for islands corresponding to different resonances. See Anderson[20] for an explanation of resonance as it is used in this paper or Murray and Dermott[26] and Szebehely[25] for more detailed explanations.

Invariant Manifolds

The invariant manifolds of resonant orbits are computed for each orbit to locate and calculate the homoclinic and heteroclinic connections used in this analysis. Briefly, the stable (unstable) manifolds may be thought of as the trajectories that approach the unstable periodic orbit in question as the time goes toward infinity (negative infinity). More formally, the stable and unstable manifolds for a flow ϕ_t are

Stable Manifold $W^s(L)$: The set of points x such that $\phi_t(x)$ approaches L as $t \to \infty$.

Unstable Manifold $W^u(L)$: The set of points x such that $\phi_t(x)$ approaches L as $t \to -\infty$.

An offset of approximately 1×10^{-6} dimensionless units is used to globalize the invariant manifolds in the majority of the computations made in this analysis.[27] In the Jupiter-Europa system this value corresponds to approximately 0.671 km. See Parker and Chua[28] for more details on invariant manifolds.

Heteroclinic and homoclinic trajectories are an essential part of this analysis, and they are computed from intersections of the stable and unstable manifolds. Mathematically, a heteroclinic trajectory is a point that belongs to

$$W^s_{a:b} \cap W^u_{c:d} \tag{5}$$

where in the notation used here, a:b and c:d designate the resonant orbit used to compute the manifolds. For this heteroclinic connection, the trajectory travels backward in time asymptotically along the unstable manifold to one resonant orbit and asymptotically forward in time along the stable manifold to the other resonant orbit. For a homoclinic trajectory a point is found that belongs to

$$W^s_{a:b} \cap W^u_{a:b}, \tag{6}$$

and the trajectory approaches the same unstable resonant orbit asymptotically both forward and backward in time.

Poincaré Sections

Poincaré maps are useful for studying complicated systems because they bring out information that would otherwise be obscured.[29] In order to compute a Poincaré map for a system in $\mathbb{R}^n$, a *hypersurface* Σ or surface of section in $\mathbb{R}^{n-1}$ is placed transverse to the flow. A trajectory intersecting the surface of section is integrated until it intersects the surface of section once again. The mapping is from the first intersection to the next intersection and so on. The points of the mapping may then be plotted using a number of different coordinates, although only some coordinates will result in visible structure. Given the planar CRTBP in $\mathbb{R}^4$, the surface of section is specified by fixing one of the coordinates in order to produce a surface in $\mathbb{R}^3$.

In this analysis, the surface of section is specified by $y = 0$ along the x-axis opposite Europa (see Fig. 9(a)). The Jacobi constant is fixed for all the points in the Poincaré section, which means that the resulting surface of section is two-dimensional. So with x defined, $\dot{x} = 0$, and $y = 0$. The magnitude of $\dot{y}$ can then be calculated in the planar problem from the Jacobi constant as

$$\dot{y} = \pm\sqrt{x^2 + y^2 + \frac{2(1-\mu)}{r_1} + \frac{2\mu}{r_2} - \dot{x}^2 - C}. \tag{7}$$

As mentioned previously, resonant orbits and their invariant manifolds are of particular importance to this analysis, and their intersections with the surface of section are computed throughout this paper. For this analysis, only those points crossing the surface of section with a positive $\dot{y}$ are plotted unless otherwise indicated. A Runge-Kutta Fehlberg seventh-order integrator with stepsize control is used to generate the Poincaré sections.

Once the information for each intersection has been recorded, the question arises as to which quantities should be plotted. With y always zero it is often useful to plot x and $\dot{x}$. Other quantities found to be helpful are the Delaunay variables[14] L and $\bar{g}$. L is the square root of the semimajor axis, and $\bar{g}$ is the argument of periapse relative to the rotating x-axis. L was useful here in selecting a point with the desired initial conditions to aid in the location of unstable resonant orbits. Using the two-body equations and an estimation of the desired period of the orbit, a relationship between L and the resonance can be found according to

$$\frac{p}{q} = \frac{n_p}{n_q} = \frac{T_q}{T_p} = \frac{\sqrt{\frac{{a_q}^3}{\mu_G}}}{\sqrt{\frac{a_p^3}{\mu_G}}} \approx {a_p}^{-3/2} = L^{-3}. \tag{8}$$

Here, μ_G is the gravitational parameter of the primary.

Differential Correction

A single shooting method was used to aid in finding the resonant orbits used in this study. The basic algorithm, described by Howell,[30] was modified for the planar case. It uses the symmetry about the x-axis in the CRTBP mentioned earlier to search for periodic orbits. Given this symmetry, a trajectory that intersects the x-axis twice with a velocity perpendicular to the x-axis will be periodic. Modifications were incorporated into the algorithm to allow for the fact that the first intersection with the x-axis is not necessarily the desired intersection for some resonant orbits. The instability of the orbits used for this study puts a lower limit on the error of approximately 10^{-11} for the single shooting technique.[31] A two-level, multiple-shooting differential corrector was used to obtain the final trajectories across multiple resonances produced as a result of this study.[32,33] Constraints were added to the differential corrector to allow the initial and final points to remain fixed.

SUMMARY OF RESONANT ORBITS

Our previous work[18–24] focused on analyzing the 3:4 and 5:6 resonances because they had been found to be key to the endgame design for a Europa mission.[5] Of course, many other unstable resonant orbits exist that possess invariant manifolds that can potentially be used to connect the various resonances. Some of these orbits of use in this study are summarized here.

In Anderson[23] resonant orbits were computed by starting from an initial guess derived from two-body approximations. A grid search was made in position and velocity around this initial guess with each initial guess used as initial conditions in a single-shooting algorithm. The resulting trajectories were then sorted to select the unstable resonant orbits based on the maximum eigenvalue of the monodromy matrix. Modifications were made to the single-shooting algorithm to allow different numbers of intersections of the resonant orbit in the search. The resonant orbits presented here were computed using these techniques and then selected from the resulting database of orbits based on their period and a final visual inspection. For easy comparison with previous work, the orbits shown here are given for the Jupiter-Europa system at an energy denoted by C_{flyby} = 2.99163956830415. The C_{flyby} energy was selected as the energy where a flyby trajectory exists that cycles between the 3:4 and 5:6 resonances in Anderson.[23] These resonant orbits may be continued in energy to obtain a family of orbits for a given system or in μ to obtain the resonant orbits in a different system. The Jacobi constants computed at the Lagrange points in the Jupiter-Europa system are listed here to place the C_{flyby} value in context.

$$\begin{aligned} C_{L_1} &= 3.00364148662088 \\ C_{L_2} &= 3.00360779675688 \\ C_{L_3} &= 3.00002526643555 \\ C_{L_4}, C_{L_5} &= 2.99997473418954 \end{aligned} \tag{9}$$

A trajectory at the C_{flyby} energy is able to travel throughout the system as the Jacobi constant is just below the point where the forbidden regions exist.

Table 1. Unstable resonant orbit characteristics at C_{flyby}. The maximum eigenvalue of the monodromy matrix is used to compare the stability of the orbits.

Resonant Orbit	Maximum Eigenvalue	$\mathbb{P}_{sc}/\mathbb{P}_e$	Period (days)
2:3	125.1	3.03	10.76
7:10	846.7	10.05	35.69
5:7	852.3	7.06	25.07
3:4	1036.1	4.09	14.51
7:9	3559.0	9.11	32.36
5:6	4445.4	6.17	21.91

The resonances chosen for analysis in this study were the 2:3, 7:10, 5:7, 3:4, 7:9, and 5:6 resonances where they are listed in order as they come closer to resonance with Europa. The selected resonant orbit families for each resonance were computed, and the trajectories at C_{flyby} in the Jupiter-Europa system are plotted in Figure 1. Note that other orbits near these resonances may exist with similar periods as was observed in Anderson,[23] but these were selected based on a combination of their locations relative to each other and their stability characteristics. Examining the orbits, one of the most obvious features in the plots is the loops along each orbit. These loops correspond to the periapse passages, where the orbit is actually traveling faster than the rotating frame. This feature can be used to determine the number of periapses along the resonant orbit over a complete revolution in the rotating frame. Additionally, it is worth noting that they do not all intersect the surface of section with a velocity normal to the surface of section as was the case in previous studies. This difference required modifications of the single-shooting code and a careful selection of initial guesses to compute the orbits. A wide variety of initial conditions and orbit types were chosen, and then the resulting periodic orbits were analyzed to select potentially useful orbits. Their specific characteristics are listed in Table 1. The most obvious trend from the characteristics of the orbits is that the maximum eigenvalue of the monodromy matrix increases as the resonance comes closer to 1:1. The periods, as would be expected with the three-body influences included, are not exactly integer ratios, but they remain relatively close to the integer value. In determining the resonance from the computed orbit, two factors may be used: the number of periapses found when plotting the periodic orbit, and the ratio of the periods ($\mathbb{P}_{sc}/\mathbb{P}_e$). These parameters

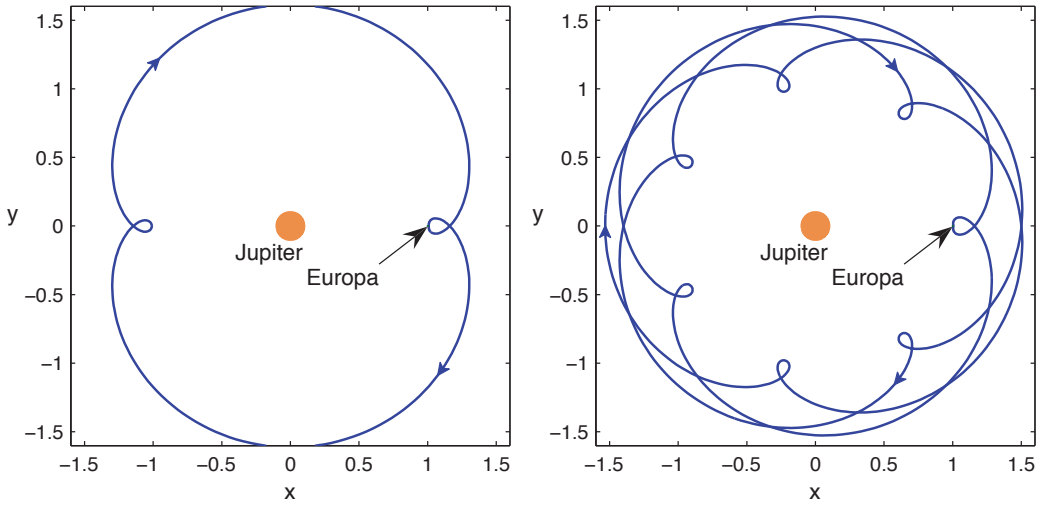

(a) 2:3

(b) 7:10

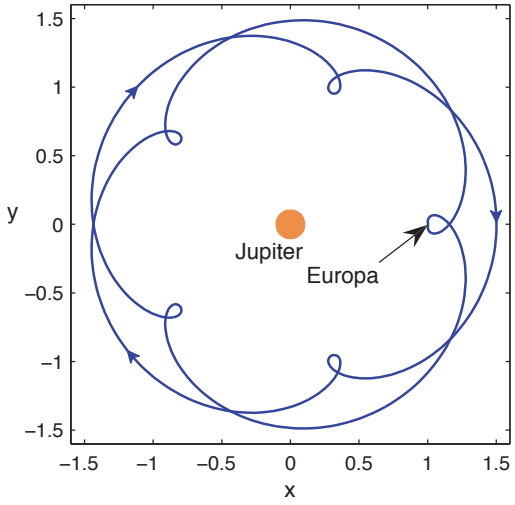

(c) 5:7

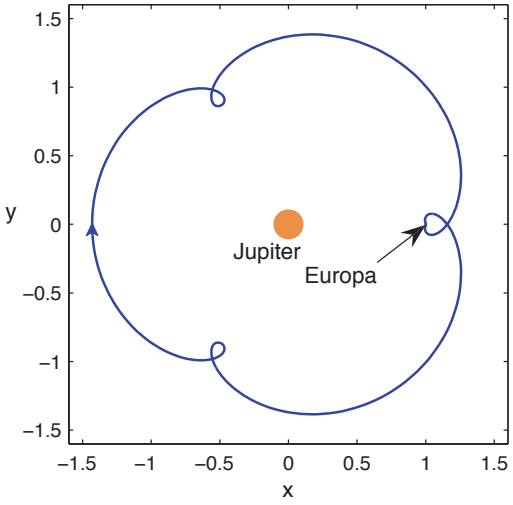

(d) 3:4

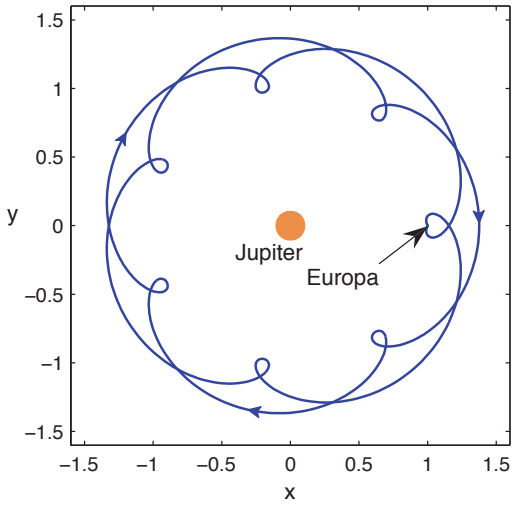

(e) 7:9

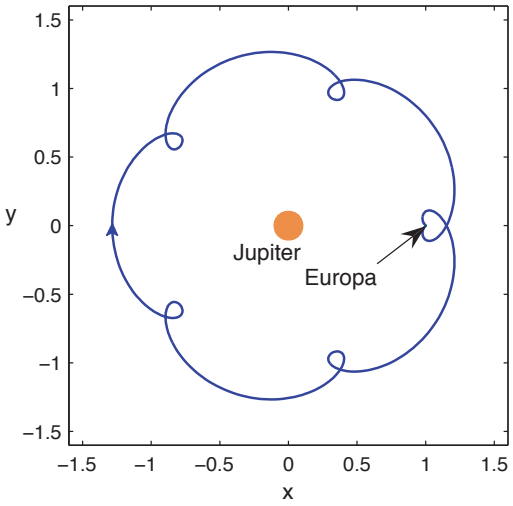

(f) 5:6

Figure 1. Resonant orbits computed for each resonance at C_{flyby}

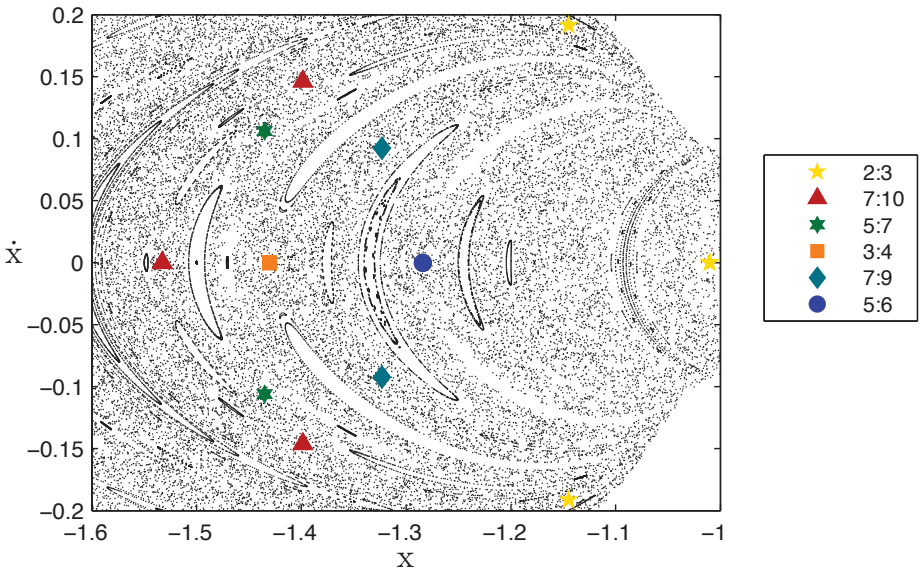

Figure 2. Poincaré section using x and $\dot{x}$ coordinates showing the resonant orbit intersections with the $y = 0$ line shown in Figure 9(a). One of the 2:3 orbit intersections has $\dot{y} < 0$ since it is at periapse.

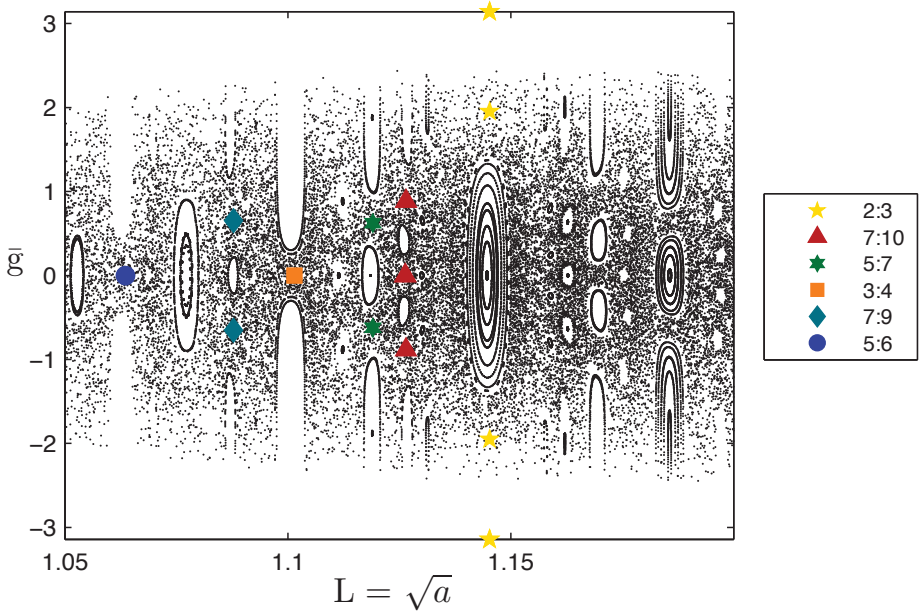

Figure 3. Poincaré section using L and $\bar{g}$ corresponding to the resonant orbit intersections in Figure 2. The resonances correspond to particular values of L in this plot. Note that the intersections at $\pm\pi$ for the 2:3 resonance are the same point.

give the number of orbits the spacecraft has traveled through in the inertial frame and the number of revolutions of Europa in the inertial frame in the same time period.

While the resonant orbits are easily viewed in plots in the xy plane, when the invariant manifolds are computed, viewing the trajectories quickly becomes very complicated with this method. A solution to this problem used in our past work[20,22] is to plot the intersection of the orbits and their invariant manifolds with the surface of section defined earlier. The intersections of the orbits in Figure 1 with the surface of section are plotted using x and $\dot{x}$ coordinates in Figure 2. The advantage of using these coordinates is that C = $f(x, y, \dot{x}, \dot{y})$ in the planar problem so that with x and $\dot{x}$ taken from the plot with $y = 0$, $\dot{y}$ can be computed from Equation 7. One interesting observation from this plot is that the 3:4 and 5:6 orbits analyzed in the previous studies intersect this surface of section only once. The 2:3 orbit intersects once at periapse, so it is the only point in the plot with a $\dot{y}$ in the negative direction. Otherwise the Poincaré map is a one-sided Poincaré map with $\dot{y} > 0$. The 7:10, 5:7, and 7:9 orbits require several revolutions in the rotating frame to repeat as can be seen from Figure 1, while the remaining orbits repeat every revolution. The non-perpendicular crossings of the orbits at the given surface of section produce the nonzero $\dot{x}$ values seen with some of the orbits in the Poincaré section. These points would, of course, change for different selections of surface of sections.

The state can be easily computed from the x, $\dot{x}$ plot, but it is not as clear which resonance the orbit intersections correspond to. This issue can be remedied by plotting the intersections using L and $\bar{q}$ as shown in Figure 3. In this plot, L is a function of the semimajor axis, and three-body perturbations are at a minimum given that the trajectory is opposite Europa for this surface of section. Indeed, this is one of the reasons for selecting this surface of section. Using these coordinates, the resonant orbits line up vertically on the plot, and as L is changed, the resonance changes.

HOMOCLINIC CONNECTIONS

The homoclinic connections observed here travel away from an unstable resonant orbit along the unstable manifold of that orbit and then return to the same orbit via the stable manifold. If the homoclinic connection is chosen from an intersection near another resonance, the trajectory undergoes a resonance transition during this process. A homoclinic connection for the 3:4 to 5:6 orbit case was computed previously in Anderson.[23] Two additional homoclinic connections are computed and shown here where the homoclinic connections are chosen so that the trajectory travels on the unstable manifold of one resonant orbit to a point near another resonant orbit. The trajectory then returns back to the original resonant orbit along its stable manifold. In this manner, the trajectory travels approximately from one resonance to another and returns via flybys of the secondary. This process first required the computation of the stable and unstable manifolds of the selected resonant orbit along with the intersections of the manifolds with the surface of section. The appropriate intersection was then selected from the Poincaré section.

The first orbit selected for analysis here was the 2:3 orbit. The Poincaré section computed for this orbit including the invariant manifolds of the 2:3 orbit and the intersections of the orbits at the 2:3 resonance and the 7:10 resonance are shown in Figure 4(a). As can be seen from the inset, the invariant manifolds of the 2:3 orbit intersect just to the left of the 7:10 resonant orbit. The points along the manifold were used to find a more precise value for the intersection using interpolation. The complete state in phase space was then computed from the known x, $\dot{x}$, and $\dot{y}$ along with the Jacobi constant. The complete trajectory shown in Figure 6(b) is integrated from an initial point on the 2:3 orbit to the homoclinic connection computed from the Poincaré section to the final point back at the 2:3 orbit. The initial and final points are not at precisely the same location because they will wind asymptotically back onto the orbit over time. It is useful though that they both come very near the 2:3 resonant orbit with only one flyby of the secondary. This fact can be more clearly seen by examining the individual segments of the trajectory. The trajectory segments divided up into parts by the computed homoclinic connection point are shown in Figure 5. It can be seen that in each case the trajectory travels one revolution around the system without a close flyby and one revolution with a close flyby.

A similar process was performed to compute a homoclinic connection for the 7:9 orbit as well. A Poincaré

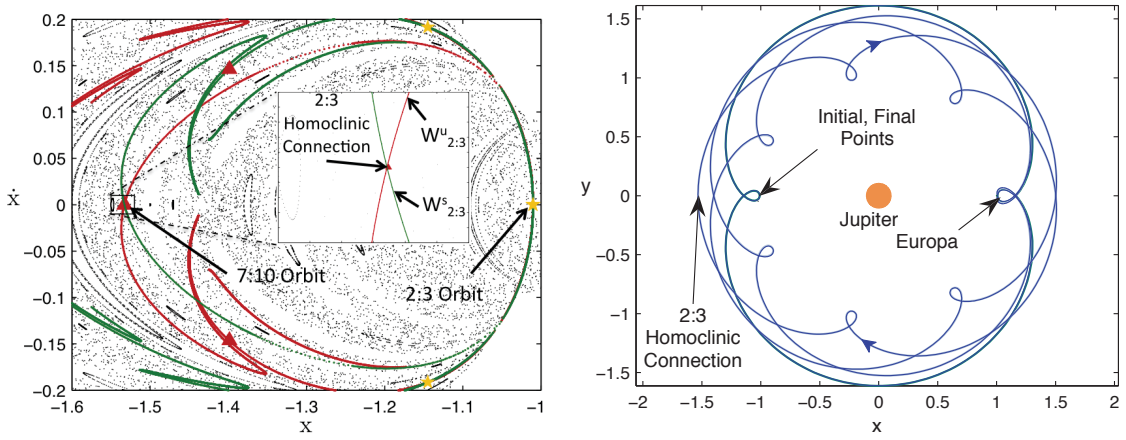

(a) Poincaré section showing homoclinic connection.

(b) Integrated trajectory computed from homoclinic connection.

Figure 4. Overview of a homoclinic connection for the 2:3 orbit.

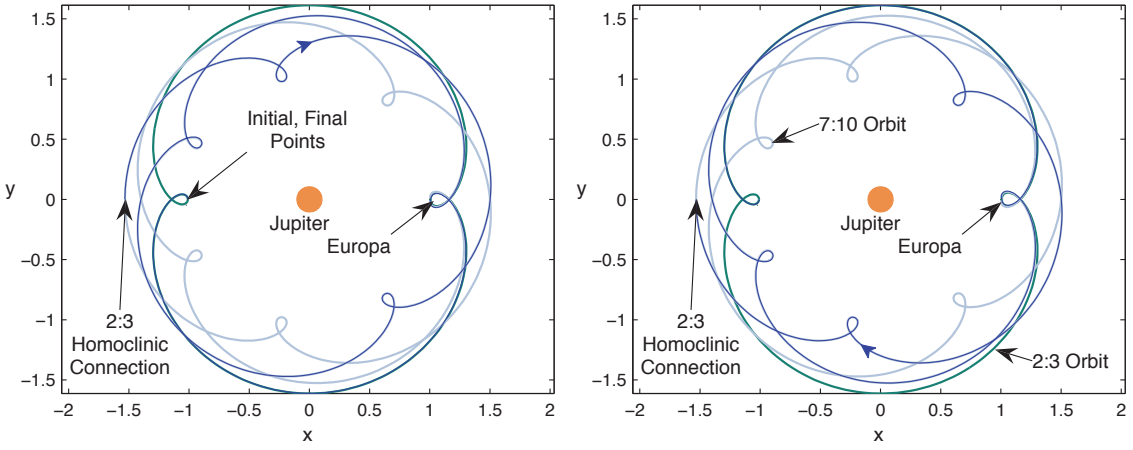

(a) Forward Integration

(b) Backward Integration

Figure 5. Segments of the homoclinic connection for the 2:3 orbit. Plots of the 7:10 and 2:3 resonant orbits are included for comparison. The trajectory is shown in blue in each plot.

section including the invariant manifolds was computed once again (omitted here for sake of space), and the segments of the resulting trajectory are shown in Figure 6 including the 3:4 and 7:9 resonant orbits. For this case, a connection near the 3:4 resonance was selected. As can be seen from the plot, the trajectory travels from the 7:9 orbit toward the 3:4 orbit and then returns to the 7:9 orbit. In this case the trajectory endpoints were not computed to the same vicinity, but they approach the 7:9 orbit at different locations.

The homoclinic connections computed for these trajectories and others demonstrate how the resonant orbit's invariant manifolds can undergo resonance transitions away from and back to particular resonances. This is analogous to rotating the V_∞ vector back and forth on successive flybys using the two-body approximations. These connections are relatively common as they have been found for these orbits in addition to others, and each orbit has multiple potential connections.

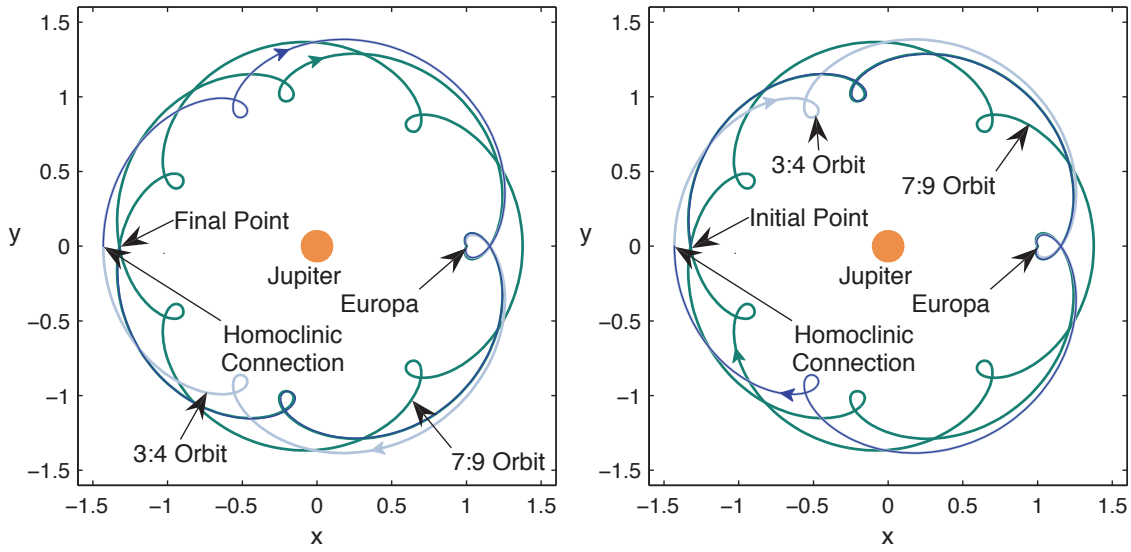

(a) Forward Integration

(b) Backward Integration

Figure 6. Segments of the homoclinic trajectory for the 7:9 orbit. Plots of the 3:4 and 7:9 resonant orbits are included for comparison. The trajectory is shown in blue in each plot.

HETEROCLINIC CONNECTIONS

The computation of trajectories employing heteroclinic connections follows a process similar to that used for homoclinic connections except that the stable and unstable manifolds of two or more resonant orbits are used. The existence of a single heteroclinic connection between two resonances was demonstrated previously in Anderson and Lo,[24] and this analysis explores multiple additional resonances for the existence of new heteroclinic connections. The potential for applications to tour design is analyzed by connecting sequences of resonances and examining the computation of heteroclinic connections for different energies. The resulting trajectories are then differentially corrected to examine the feasibility of this method for computing continuous tours using flybys.

The process employed in this analysis may be briefly summarized using a spacecraft approaching Europa from an outer resonance with an initial period greater than that of Europa's. In this case, a sequence of resonances may be selected, and the resonant orbits at a particular Jacobi constant may all be computed. The corresponding stable and unstable manifolds of each orbit are also computed, and their intersections with the selected surface of section are retained. A search may then be made for heteroclinic connections by noting where the invariant manifolds of the selected resonant orbits intersect. In particular, the locations where the unstable manifolds of the initial resonant orbit intersect with the stable manifolds of a resonant orbit possessing a resonance closer to Europa are selected. In the PCRTBP, the state on the heteroclinic connection may be computed from the intersection in the Poincaré section, and integrations forward and backward may be made. The backward integrated state approaches the initial resonant orbit along its unstable manifold, and the forward integrated state approaches the next resonant orbit along its stable manifold. These trajectories will approach their respective resonant orbits asymptotically, so the trajectories are computed only until they come close to the resonant orbits. The trajectories analyzed here typically approach the resonant orbit closely after a single flyby of the secondary. To compute transitions across multiple resonances, several heteroclinic connections are computed while selecting the intermediate resonant orbits so that they match. If the trajectories are allowed to wind asymptotically onto their respective orbits, the final trajectory computed from this chain would theoretically have no required deterministic ΔV. Practically, though, the endpoints of each heteroclinic trajectory are computed when they come close to the resonant orbit and are connected to

the next heteroclinic trajectory with a small discontinuity. In the final step, a differential corrector is applied to the heteroclinic chain to search for a continuous trajectory.

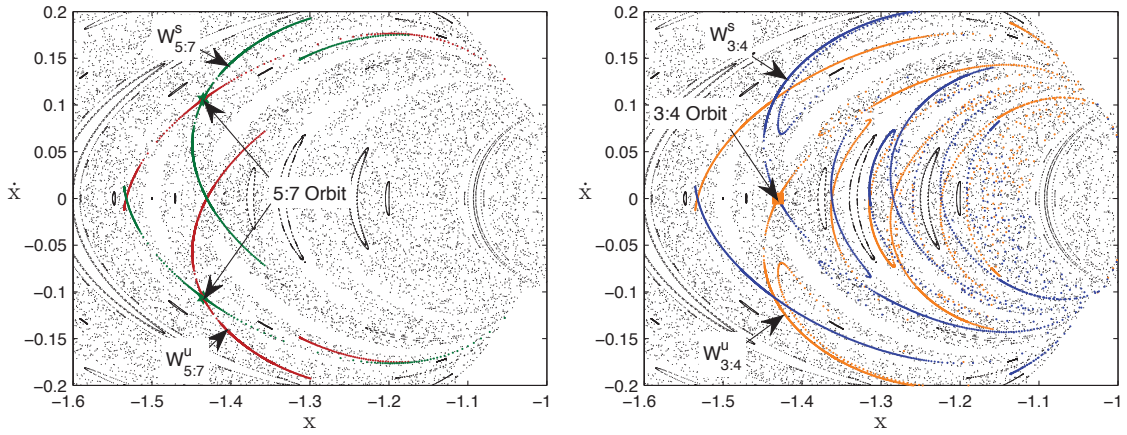

(a) 5:7 orbit invariant manifolds

(b) 3:4 orbit invariant manifolds

Figure 7. Poincaré sections for the 5:7 and 3:4 orbits shown separately at C_{flyby}.

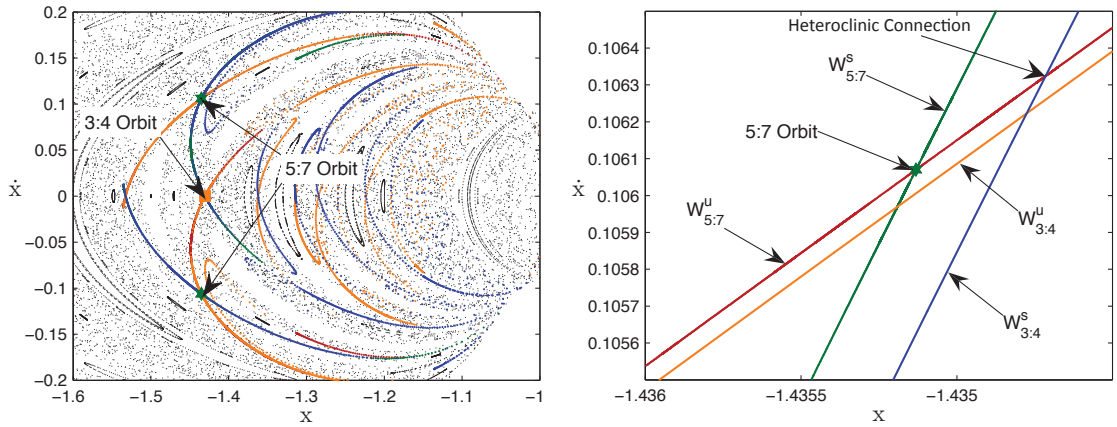

(a) Overview including orbits and manifolds

(b) Close view around the upper 5:7 intersection

Figure 8. Poincaré section including the stable and unstable manifolds of both the 5:7 and 3:4 orbits at C_{flyby}.

The process described above is applied to a particular case with a detailed explanation here, and then it is applied to several other instances to begin to explore the potential design space. For this initial case, heteroclinic connections traversing the 5:7, 3:4, and 5:6 resonances at C_{flyby} are computed and then connected. The first step requires finding a suitable heteroclinic connection between the 5:7 and 3:4 resonant orbits. To search for this connection, the invariant manifolds of the 5:7 and 3:4 orbits were computed and plotted as shown in Figure 7. As can be seen from these plots, the invariant manifolds of both orbits have very similar characteristics and travel to some of the same resonances. Indeed, if the invariant manifolds are plotted in the same plot as given in Figure 8(a), it can be seen that the invariant manifolds almost overlap. Examining the invariant manifolds more closely as in Figure 8(b), it is clear that the invariant manifolds are slightly offset. However, it can be seen from the figure that the unstable manifold of the 5:7 orbit (the initial resonance) does in fact intersect the stable manifold of the 3:4 orbit in the upper right hand corner. Although several

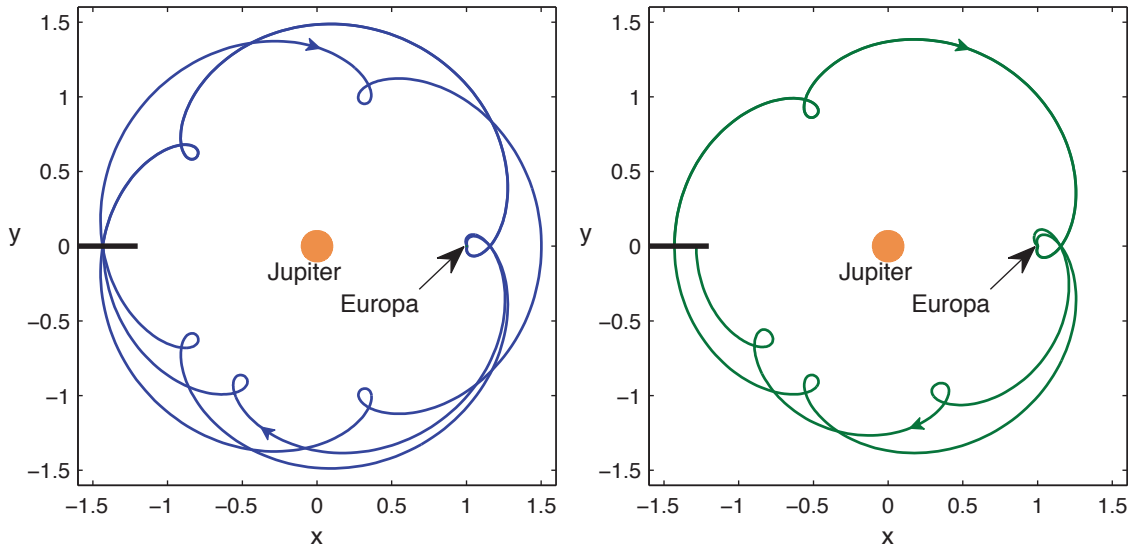

(a) Heteroclinic trajectory from 5:7 to 3:4 resonance

(b) Heteroclinic trajectory from 3:4 to 5:6 resonance

Figure 9. The heteroclinic trajectories between the 5:7, 3:4, and 5:6 resonances plotted separately.

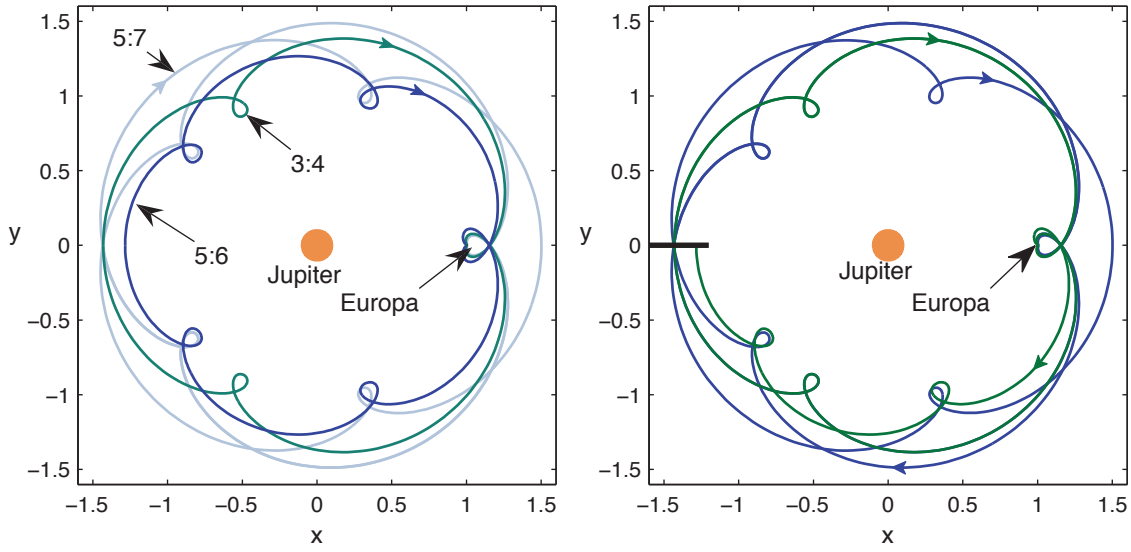

(a) Resonant orbits

(b) Heteroclinic trajectories plotted together

Figure 10. Heteroclinic trajectories plotted for comparison with the resonant orbits. The intermediate point connecting the heteroclinic trajectories occurs at the surface of section with a small discontinuity in position. The initial point on the trajectory is at the left position on the surface of section, and the final point is the furthest to the right in the surface of section.

heteroclinic connections exist, this connection was selected for study here. The connection already exists near the 5:7 orbit, and it will only approach it more closely with a backward integration. The forward integration should bring the trajectory closer then to the 3:4 orbit. The complete heteroclinic connection for this example can be seen in Figure 9(a). The backward integrated trajectory stays near the 5:7 resonance, and the

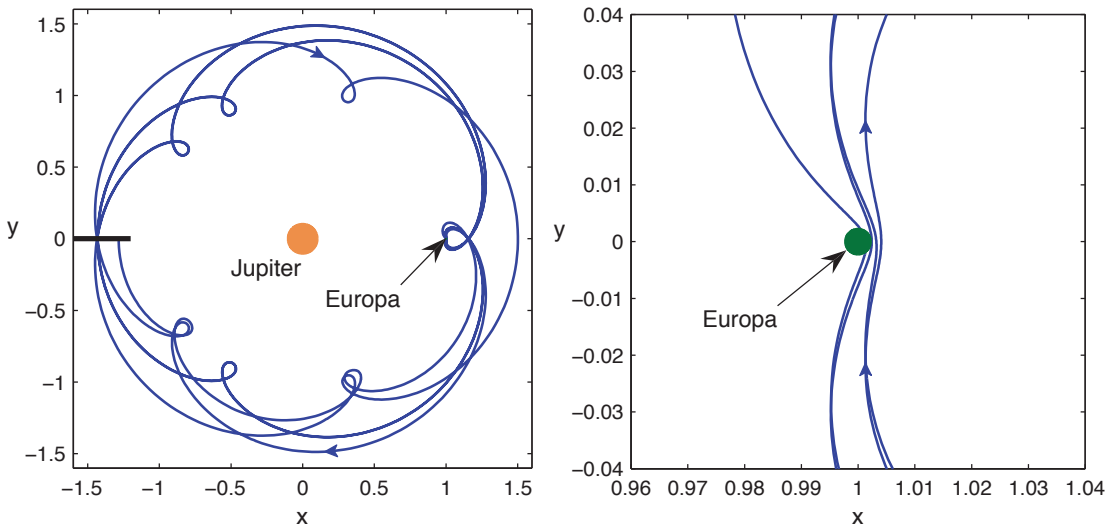

(a) Overview (b) Near Europa

Figure 11. Differentially corrected trajectory with the endpoints constrained traveling in order between the 5:7, 3:4, and 5:6 resonances.

Table 2. Europa close approach parameters computed relative to Europa. (5:7, 3:4, 5:6 case) r_p **and** v_p **are the periapse radius and velocity with respect to Europa, and** E_p **is the two-body energy with respect to Europa at that point.**

Time (days)	r_p (km)	$v_p(m/s)$	E_p (km^2/s^2)
6.9	2754.7	2029.5	0.897
31.9	2162.4	2171.7	0.878
46.4	1628.0	2377.5	0.860
60.9	960.7	2887.5	0.837

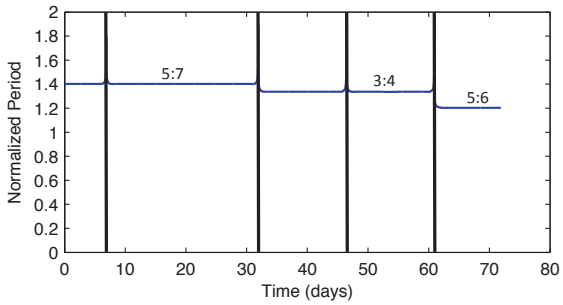

Figure 12. The two-body period of the trajectory in Figure 11 normalized by Europa's period. The vertical lines mark flybys of Europa.

forward integrated trajectory approaches the 3:4 resonance. In this case, the position at the crossing of the particular surface of section does not change significantly, but the orbits have obviously changed shape. The velocity orientation is also quite different. For the next case, a similar process was performed to compute a heteroclinic connection between the 3:4 and 5:6 resonant orbits. In this case, the change in resonance is even

clearer compared to the surface of section as the intersection starts initially on the left side of the surface of section and ends up on the right as shown in Figure 9(b). The chain of heteroclinic connections from the 5:7 to the 3:4 resonance and from the 3:4 resonance to the 5:6 resonance are plotted together in Figure 10(b). Comparing with the plots of the resonant orbits in Figure 10(a), it can be seen that the heteroclinic trajectories have moved from near the shape of the 5:7 orbit to the shape of the 5:6 orbit, and the trajectory has moved in position from left to right in the surface of section.

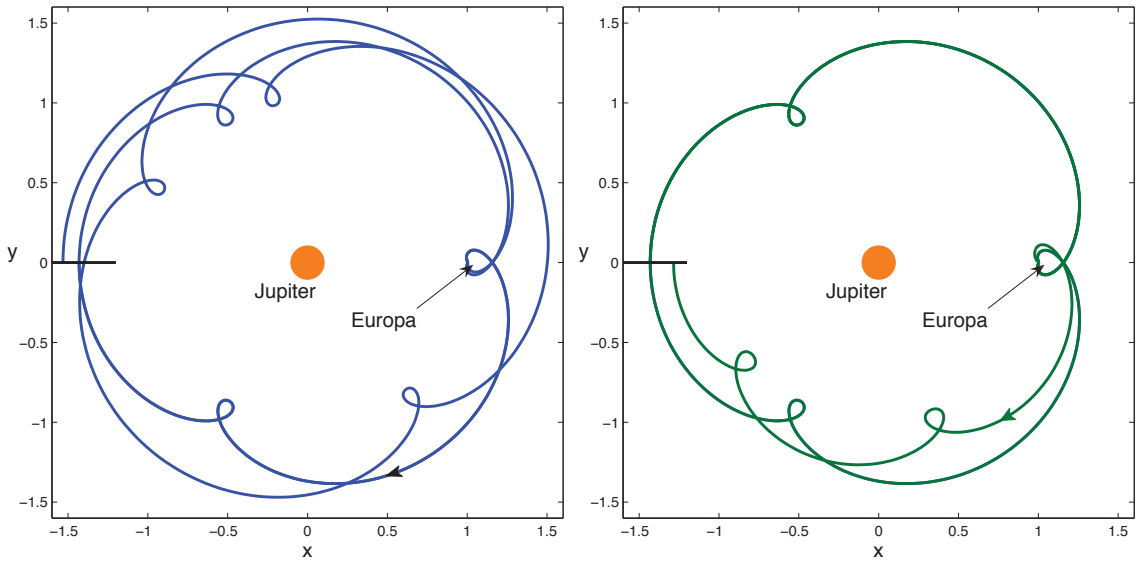

(a) Heteroclinic trajectory from 7:10 to 3:4 resonance

(b) Heteroclinic trajectory from 3:4 to 5:6 resonance

Figure 13. The heteroclinic trajectories between the 7:10, 3:4, and 5:6 resonances plotted separately.

One of the objectives of this analysis is to evaluate the potential use of these heteroclinic connections to hop between multiple resonances without requiring them to fully wind on to each orbit. This application was examined here by connecting the heteroclinic connections once they had come close to the orbit as they intersected the surface of section. The resulting trajectory, including the segments for each heteroclinic connection, was then placed in a differential corrector, keeping the endpoints constrained in position. For this initial case, a total of 50 patchpoints were used, which produced the trajectory shown in Figure 11. The sum of the position differences at the patchpoints for this trajectory is 1.7 m, and the sum of the velocity differences is 0.000041 m/s. The time of flight (TOF) for the entire trajectory is 71.9 days, and the flyby parameters are listed in Table 2. The resonances the trajectory travels through over time may be seen by examining the plot of the period of the trajectory over time in Figure 12. Note that the last flyby passes below the surface of Europa (1560.7 km) for this trajectory. This fact is potentially useful if landing or impact trajectories at Europa are desired, but if continued resonance transitions are desired, a trajectory with different characteristics would need to be found. This will be addressed a little later in the analysis.

While this trajectory appears to be viable, an obvious question is related to whether this same technique is useful for connecting additional resonances. This question is approached here by examining a similar case connecting three resonances. For this case, the 5:7 resonance is replaced with the 7:10 resonance in the previous sequence. The same process for selecting the heteroclinic connections using the Poincaré sections was performed here, although the plots are omitted here for the sake of space. The resulting connections are plotted separately in Figure 13 and together in Figure 14. Here, it is easier to the see the change in resonance for the connection between the 7:10 and 3:4 resonances as the trajectory moves from left to right in the surface of section. The overall orbit moves from very near the shape of the 7:10 resonant orbit toward the shape of the 5:6 resonant orbit. A similar process as that used before was performed to differentially correct the trajectory, and the resulting orbit is shown in Figure 15. The differentially corrected trajectory in

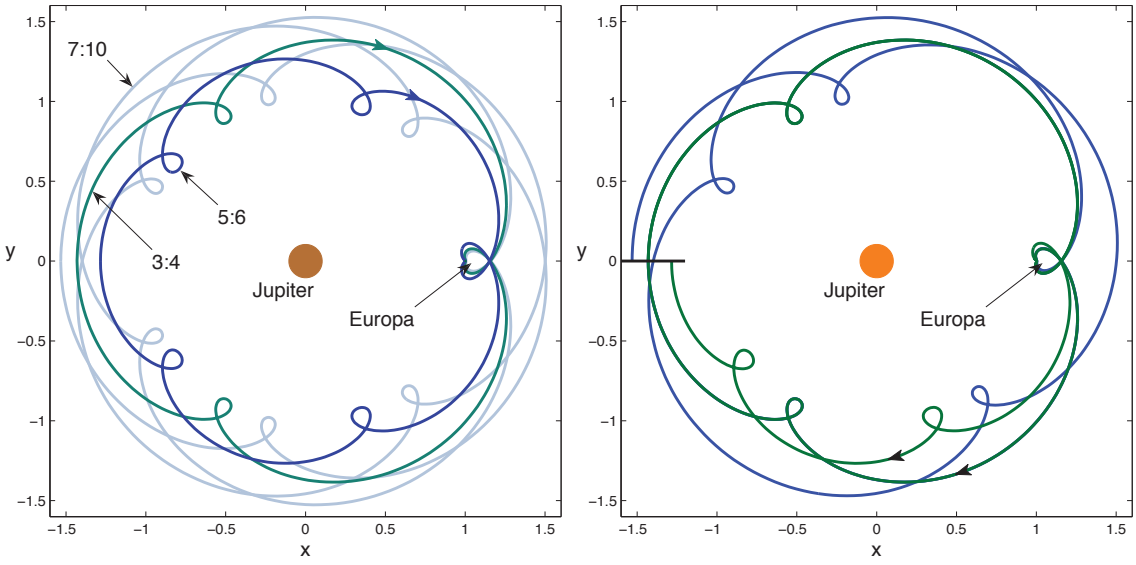

(a) Resonant orbits

(b) Heteroclinic trajectories plotted together

Figure 14. Heteroclinic trajectories plotted for comparison with the resonant orbits. The intermediate point connecting the heteroclinic trajectories occurs at the surface of section with a small discontinuity in position.

this case had a total position difference of approximately 3.08 m, and a velocity difference of 0.000066 m/s. The specific characteristics of this trajectory are given in Table 3. Once again, the trajectory passes below the surface of Europa because the same heteroclinic connection between the 3:4 and 5:6 orbits was used for this sequence.

Table 3. Europa close approach parameters computed relative to Europa. (7:10, 3:4, 5:6 case)

Time (days)	$r_p\ (km)$	$v_p(m/s)$	$\mathrm{E}_p\ (km^2/s^2)$
17.8	2489.5	2085.2	0.888
32.4	1630.2	2376.8	0.860
46.9	1628.8	2377.0	0.860
61.4	961.5	2886.5	0.837

Table 4. Europa close approach parameters computed relative to Europa. (5:7, 3:4, 7:9, 5:6 case)

Time (days)	$r_p\ (km)$	$v_p(m/s)$	$\mathrm{E}_p\ (km^2/s^2)$
6.9	2733.9	2034.9	0.900
31.9	2144.6	2178.3	0.880
46.4	1615.4	2385.0	0.862
60.9	1328.0	2554.6	0.853
93.3	1304.1	2571.5	0.852

One possible way of avoiding this situation might involve inserting an intermediate resonant orbit between

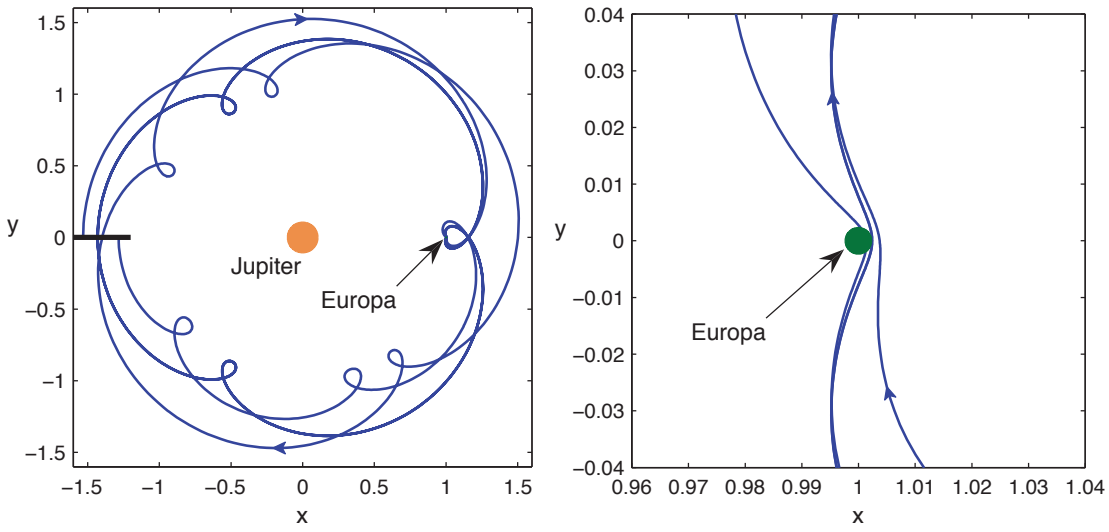

(a) Overview (b) Near Europa

Figure 15. Differentially corrected trajectory with the endpoints constrained traveling in order between the 7:10, 3:4, and 5:6 resonances.

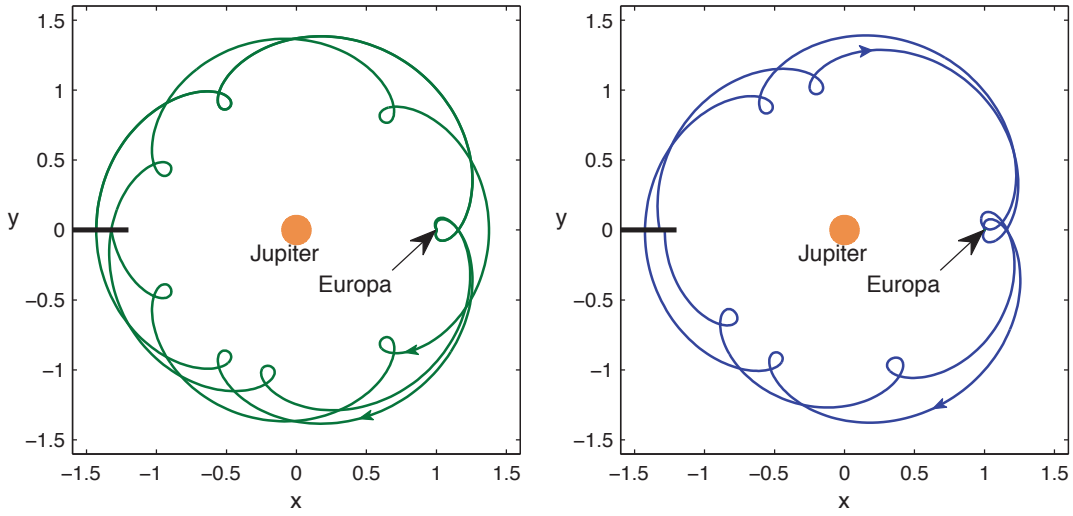

(a) Heteroclinic trajectory from 3:4 to 7:9 resonance (b) Heteroclinic trajectory from 7:9 to 5:6 resonance

Figure 16. The heteroclinic trajectories between the 3:4, 7:9, and 5:6 resonances plotted separately.

the 3:4 and 5:6 resonances. This possibility is examined here by looking at a sequence traversing the 5:7, 3:4, 7:9, and 5:6 resonances in that order. For this sequence, the same trajectory traveling from the 5:7 to the 3:4 resonance was used. The trajectories computed from the heteroclinic connections between the 3:4, 7:9, and 5:6 resonances are shown in Figure 16. An overview containing all the segments of the trajectory together is given in Figure 17, and the differentially corrected version of the trajectory is shown in Figure 18. Some more time was spent refining this trajectory using the differential corrector, and the final result contained 10 patchpoints with a total position difference of 2.3737 m and a total velocity difference of 0.000028 m/s. Specific details of this trajectory are listed in Table 4. Unfortunately, at this energy the trajectory still travels

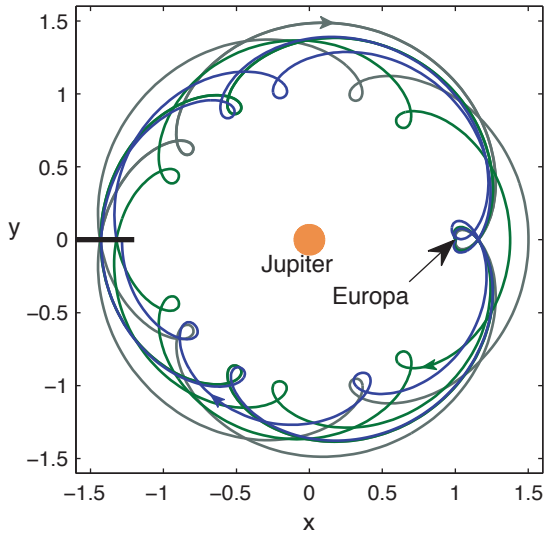

Figure 17. The heteroclinic trajectories between the 5:7, 3:4, 7:9, and 5:6 resonances plotted together.

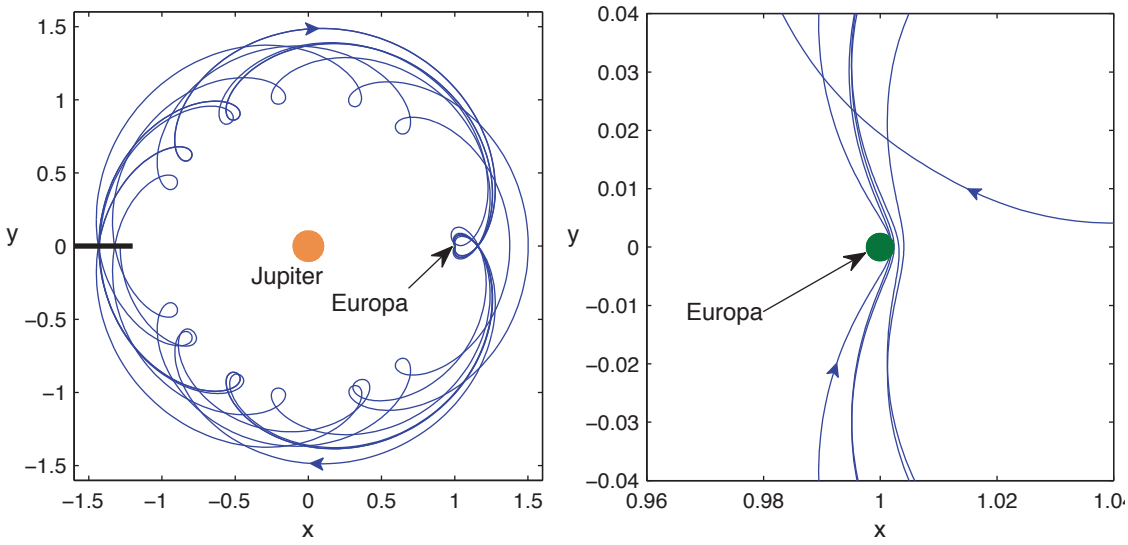

(a) Overview (b) Near Europa

Figure 18. Differentially corrected trajectory with constrained endpoints traveling in order between the 5:7, 3:4, 7:9, and 5:6 resonances.

underneath the surface of Europa as it transitions through the resonances.

This occurrence does not affect the validity of the theory and its potential applications in a wide variety of situations. It simply indicates that a different energy is required to perform this resonance transition given the constraint of flying above Europa's surface. In each of the cases examined so far, the incursion below the surface of Europa has occurred during the transition process from the 3:4 to the 5:6 resonance. It is interesting to examine a case for a different Jacobi constant to determine whether the trajectory will remain above the surface for this resonance transition. Several cases have been examined, but a useful example may be taken from the analysis of the planar Europa orbiter in Anderson and Lo.[20] For this case, a resonance transition was

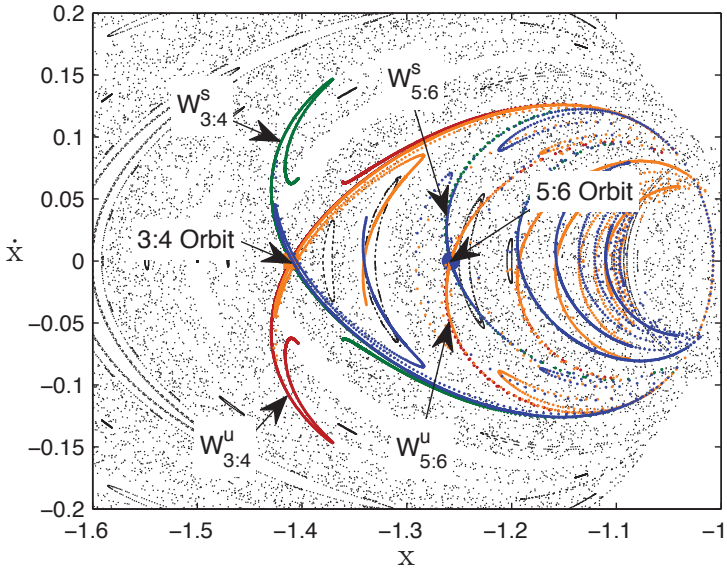

Figure 19. Poincaré section showing the manifolds for the 3:4 and 5:6 resonant orbits at C_m.

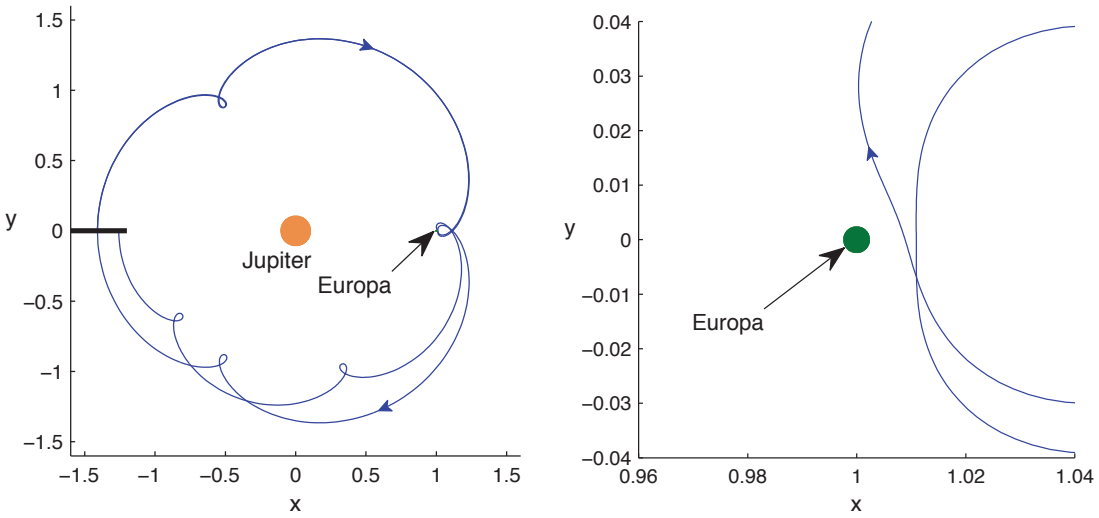

(a) Overview (b) Near Europa

Figure 20. Heteroclinic connection between the 3:4 and 5:6 resonant orbits at C_m.

known to occur for a Jacobi constant of C_m = 2.99742497175. This energy was selected and analyzed for the resonance transition from 3:4 to 5:6 here. The orbit and invariant manifold intersection with the surface of section for the two resonances are shown in Figure 19. It is interesting to note that the previous study showed that the invariant manifolds of the 5:6 orbit did not travel back to the 3:4 orbit for a Jacobi constant of C = 3.00245952365. For the C_m Jacobi constant, the invariant manifolds no longer lie nearly on top of each other as seen at C_{flyby}, but heteroclinic connections still do exist at this energy. A heteroclinic connection near the 3:4 orbit was selected for further analysis here, and the resulting trajectory for this connection is shown in Figure 20. This trajectory remains well above the surface of Europa and could be used as part of another

heteroclinic chain of trajectories to transition between multiple resonances. Specifically, the two flybys occur at radii of 5669.6 km and 7345.1 km, respectively. The fact that a change in the Jacobi constant can produce such an effect indicates that selecting the proper energy is an important aspect of computing these heteroclinic connections in the resonance transition design process.

CONCLUSIONS

For this analysis, several single homoclinic and heteroclinic trajectories traveling across resonance transitions have been successfully found and computed in the CRTBP. Multiple heteroclinic connections have been chained together and differentially corrected to form feasible trajectories going through multiple resonances at a particular energy. The resulting trajectories required very minimal ΔV to traverse the selected resonances at this particular energy. It was further demonstrated that an additional resonance transition could be inserted into the sequence to successfully raise the periapse for the flyby of Europa. It was then shown that a change in the energy could alter the characteristics of the trajectory, specifically to raise the flyby close approach above the surface of Europa. The application of these techniques shows that they successfully provide an alternative method of visually or geometrically computing gravity flybys from the invariant manifolds of unstable resonant orbits in the full CRTBP.

FUTURE WORK

Future work will include analysis of additional resonance transitions over different Jacobi constants. Interior resonances will be examined for trajectories coming from different initial conditions. Additional differential correction techniques will be employed, especially with constraints for different mission design parameters. It is anticipated that these trajectories will exist in the ephemeris model so additional analysis will be performed to bring the trajectories into the full ephemeris model using differential correction. Finally, combinations of CRTBP problems will be patched together to design complete tours using these methods.

ACKNOWLEDGEMENTS

The research presented in this paper has been carried out at the Jet Propulsion Laboratory, California Institute of Technology, under a contract with the National Aeronautics and Space Administration.

REFERENCES

[1] J. A. Sims and J. M. Longuski, "Analysis of V_∞ Leveraging for Interplanetary Missions," *AIAA/AAS Astrodynamics Conference*, No. AIAA-1994-3769, Scottsdale, Arizona, August 1-3 1994.

[2] S. Campagnola and R. Russell, "Endgame Problem Part 1: V-Infinity-Leveraging Technique and the Leveraging Graph," *Journal of Guidance, Control, and Dynamics*, Vol. 33, No. 2, 2010, pp. 463–475.

[3] R. C. Woolley and D. J. Scheeres, "Hyperbolic Periodic Orbits in the Three-Body Problem and their Application to Orbital Capture," *AAS George H. Born Symposium*, Boulder, Colorado, May 13-14 2010.

[4] T. Sweetser, R. Maddock, J. Johannesen, J. Bell, P. Penzo, A. Wolf, S. Williams, S. Matousek, and S. Weinstein, "Trajectory Design for a Europa Orbiter Mission: A Plethora of Astrodynamic Challenges," *Advances in the Astronautical Sciences, Spaceflight Mechanics* (K. C. Howell, D. A. Cicci, J. John E. Cochran, and T. S. Kelso, eds.), Vol. 95, Part I, San Diego, California, American Astronautical Society, Univelt Inc., 1997, pp. 901–920.

[5] J. R. Johannesen and L. A. D'Amario, "Europa Orbiter Mission Trajectory Design," *Advances in the Astronautical Sciences, Astrodynamics* (K. C. Howell, F. R. Hoots, B. Kaufman, and K. T. Alfriend, eds.), Vol. 103, Part III, San Diego, California, American Astronautical Society, Univelt Inc., 1999, pp. 895–908.

[6] M. Okutsu, T. J. Debban, and J. M. Longuski, "Tour Design Strategies for the Europa Orbiter Mission," *Advances in the Astronautical Sciences, Astrodynamics* (D. B. Spencer, C. C. Seybold, A. K. Misra, and R. J. Lisowski, eds.), Vol. 109, Part III, San Diego, California, American Astronautical Society, Univelt Inc., 2001, pp. 2269 – 2284.

[7] N. J. Strange and J. M. Longuski, "Graphical Method for Gravity-Assist Trajectory Design," *Journal of Spacecraft and Rockets*, Vol. 39, January-February 2002, pp. 9–16.

[8] S. Campagnola and R. Russell, "Endgame Problem Part 2: Multibody Technique and the Tisserand-Poincare Graph," *Journal of Guidance, Control, and Dynamics*, Vol. 33, No. 2, 2010, pp. 476–486.

[9] K. W. Kloster, A. E. Petropoulos, and J. M. Longuski, "Europa Orbiter Tour Design with Io Gravity Assists," *Acta Astronautica (in press)*, 2010.
[10] E. Bollt and J. D. Meiss, "Targeting Chaotic Orbits to the Moon through Recurrence," *Physics Letters A*, Vol. 204, August 28 1995, pp. 373–378.
[11] C. G. Schroer and E. Ott, "Targeting in Hamiltonian Systems that have Mixed Regular/Chaotic Phase Spaces," *Chaos*, Vol. 7, December 1997, pp. 512–519.
[12] E. Belbruno and B. Marsden, "Resonance Hopping in Comets," *Astronomical Journal*, Vol. 113, No. 4, 1997, pp. 1433–1444.
[13] M. Lo and S. Ross, "Low Energy Interplanetary Transfers Using Invariant Manifolds of L1, L2, and Halo Orbits," *AAS/AIAA Space Flight Mechanics Meeting*, No. AAS 98-136, Monterey, California, February 9-11 1998.
[14] W. S. Koon, M. W. Lo, J. E. Marsden, and S. D. Ross, "Heteroclinic Connections between Periodic Orbits and Resonance Transitions in Celestial Mechanics," *Chaos*, Vol. 10, June 2000, pp. 427–469.
[15] K. C. Howell, B. Marchand, and M. W. Lo, "Temporary Satellite Capture of Short-Period Jupiter Family Comets from the Perspective of Dynamical Systems," *The Journal of the Astronautical Sciences*, Vol. 49, October-December 2001, pp. 539–557.
[16] G. Lantoine and R. P. Russell, "Near-Ballistic Halo-to-Halo Transfers Between Planetary Moons," *AAS George H. Born Astrodynamics Symposium*, Boulder, CO, May 13-14 2010.
[17] S. D. Ross and D. J. Scheeres, "Multiple Gravity Assists, Capture, and Escape in the Restricted Three-Body Problem," *Siam Journal On Applied Dynamical Systems*, Vol. 6, 2007, pp. 576–596.
[18] M. W. Lo, R. L. Anderson, G. Whiffen, and L. Romans, "The Role of Invariant Manifolds in Low Thrust Trajectory Design (Part I)," *Advances in the Astronautical Sciences, Spaceflight Mechanics* (S. L. Coffey, A. P. Mazzoleni, K. K. Luu, and R. A. Glover, eds.), Vol. 119, San Diego, California, American Astronautical Society, Univelt Inc., 2004, pp. 2971–2990.
[19] R. L. Anderson and M. W. Lo, "The Role of Invariant Manifolds in Low Thrust Trajectory Design (Part II)," *AIAA/AAS Astrodynamics Specialist Conference*, No. Paper AIAA 2004-5305, Providence, Rhode Island, August 16-19 2004.
[20] R. L. Anderson and M. W. Lo, "Dynamical Systems Analysis of Planetary Flybys and Approach: Planar Europa Orbiter," *Journal of Guidance, Control, and Dynamics*, Vol. 33, November-December 2010, pp. 1899–1912.
[21] M. W. Lo, R. L. Anderson, T. Lam, and G. Whiffen, "The Role of Invariant Manifolds in Low Thrust Trajectory Design (Part III)," *AAS/AIAA Astrodynamics Specialist Conference*, No. Paper AAS 06-190, Tampa, Florida, January 22-26 2006.
[22] R. L. Anderson and M. W. Lo, "Role of Invariant Manifolds in Low-Thrust Trajectory Design," *Journal of Guidance, Control, and Dynamics*, Vol. 32, November-December 2009, pp. 1921–1930.
[23] R. L. Anderson, *Low Thrust Trajectory Design for Resonant Flybys and Captures Using Invariant Manifolds*. PhD thesis, University of Colorado at Boulder, http://ccar.colorado.edu/~rla/papers/andersonphd.pdf, 2005.
[24] R. L. Anderson and M. W. Lo, "Dynamical Systems Analysis of Planetary Flybys and Approach: Ballistic Case," *The Journal of the Astronautical Sciences (submitted)*, 2011.
[25] V. Szebehely, *Theory of Orbits: The Restricted Problem of Three Bodies*. New York: Academic Press, 1967, pp. 7-41.
[26] C. D. Murray and S. F. Dermott, *Solar System Dynamics*. Cambridge, United Kingdom: Cambridge University Press, 1999, pp. 421-428.
[27] G. Gómez, A. Jorba, J. Masdemont, and C. Simó, "Study of the Transfer from the Earth to a Halo Orbit Around the Equilibrium Point L_1," *Celestial Mechanics and Dynamical Astronomy*, Vol. 56, August 1993, pp. 541–562.
[28] T. Parker and L. O. Chua, *Practical Numerical Algorithms for Chaotic Systems*. New York: Springer-Verlag, 1989, pp. 130-166.
[29] S. Wiggins, *Introduction to Applied Nonlinear Dynamical Systems and Chaos*, Vol. 2 of *Texts in Applied Mathematics*. New York: Springer-Verlag, 2nd ed., 2003, pp. 28-70.
[30] K. C. Howell and J. V. Breakwell, "Three-Dimensional, Periodic, 'Halo' Orbits," *Celestial Mechanics*, Vol. 32, January 1984, pp. 53–71.
[31] J. Masdemont and J. M. Mondelo, "Notes for the Numerical and Analytical Techniques Lectures (draft version)," Advanced Topics in Astrodynamics Summer Course, Barcelona, July, 2004, http://www.ieec.fcr.es/astro04/notes/analnum.pdf, July 2004.
[32] R. S. Wilson, "Derivation of Differential Correctors Used in GENESIS Mission Design," IOM 312.I-03-002, Jet Propulsion Laboratory, 2003.
[33] H. J. Pernicka, "The Numerical Determination of Lissajous Orbits in the Circular Restricted Three-Body Problem," Master's thesis, Purdue University, December 1986.